



Article

Process Optimization of Biodiesel Production from Waste Cooking Oil and Neem Oil Blend

Sara Maen Asaad 1,2, Abrar Inayat 1,*, Farrukh Jamil 3 and Paul Hellier 4,*

- Biomass and Bioenergy Research Group, Center for Sustainable Energy and Power Systems Research, Research Institute of Sciences and Engineering, University of Sharjah, Sharjah 27272, United Arab Emirates; u21105741@sharjah.ac.ae
- ² Department of Industrial Engineering and Engineering Management, University of Sharjah, Sharjah 27272, United Arab Emirates
- 3 Faculty of Engineering, Muscat University, Muscat 550, Oman; fjamil@muscatuniversity.edu.om
- Department of Mechanical Engineering, University College London, Torrington Place, London WC1E 7JE, UK
- * Correspondence: ainayat@sharjah.ac.ae (A.I.); p.hellier@ucl.ac.uk (P.H.)

Abstract

This study explores the use of a novel heterogeneous CoZnFe₄O₈ nanocatalyst for biodiesel production from a sustainable and innovative blend of waste cooking oil and neem oil feedstock. Utilizing waste cooking oil and inedible neem oil feedstock to produce biodiesel provides a green and economical way to produce renewable and environmentally friendly fuel while simultaneously reducing waste and valorizing inedible oils. Additionally, this feedstock blend does not threaten food or land resources as opposed to feedstocks obtained from edible resources. To fulfill the rising demand for biodiesel and address issues related to lower ester yields, particularly when utilizing waste cooking oils with high free fatty acid concentration, there is an urgent need for more effective processes, including two-stage transesterification. The novel CoZnFe₄O₈ nanocatalyst employed in this study demonstrated high efficiency in biodiesel production thanks to its high surface area, mesoporous structure, and catalytic properties. The effect of key process parameters, including catalyst concentration, reaction time, alcohol-to-oil molar ratio, and oil blend ratio, was investigated to evaluate the performance of the nanocatalyst and optimize the biodiesel yield with the help of Response Surface Methodology (RSM). The optimized process achieved a yield of 94.23% under optimum parameters of 2.13 wt% catalyst, 6.80:1 methanol-to-oil ratio, 4 h, and a ratio of waste cooking oil to neem oil of 98.32:1.68. The predicted and experimental values were in close agreement, indicating that the model was adequate. Additionally, detailed catalyst characterization, including analysis of the surface area, structure, and thermal stability, was carried out. Similarly, the biodiesel was characterized to assess its quality through heating value, density, Fourier Transform Infrared (FTIR) spectroscopy, and ultimate analysis. The recovery and reusability of the nanocatalyst were also investigated, highlighting its potential for multiple reaction cycles. The novel CoZnFe₄O₈ nanocatalyst and innovative feedstock blend demonstrated high efficiency in biodiesel production comparable to other nanocatalysts and feedstocks reported in the literature, highlighting their potential as an efficient and sustainable method to produce biofuels.

Keywords: biodiesel; response surface methodology; optimization; anova; waste oil; nanocatalyst; characterization; catalyst reusability

Academic Editor: Diego Luna

Received: 3 August 2025 Revised: 10 September 2025 Accepted: 15 September 2025 Published: 17 September 2025

Citation: Asaad, S.M.; Inayat, A.; Jamil, F.; Hellier, P. Process Optimization of Biodiesel Production from Waste Cooking Oil and Neem Oil Blend. *Energies* **2025**, *18*, 4944. https://doi.org/10.3390/ en18184944

Copyright: © 2025 by the authors. Licensee MDPI, Basel, Switzerland. This article is an open access article distributed under the terms and conditions of the Creative Commons Attribution (CC BY) license (https://creativecommons.org/license s/by/4.0/).

Energies 2025, 18, 4944 2 of 26

1. Introduction

The majority of global energy is obtained from fossil fuels, including oil, coal, and natural gas, given their high energy density and low cost. However, the cost of sustaining the anticipated growth will probably rise dramatically. As fossil fuels are a finite resource, there can be variations in how they are extracted, which can affect how much they cost [1]. Moreover, the combustion of fossil fuels results in harmful gaseous emissions [2] such as nitrogen monoxide and sulfur dioxide, which lead to a significant negative impact on the environment. Additionally, they can cause smog, harm human health, and stunt plant growth. Sulfur dioxide, in particular, causes acid rain, which can destroy crops and damage monuments [3]. The global climate is being influenced by the warming of the atmosphere caused by elevated amounts of greenhouse gases, including carbon dioxide, resulting from the burning of fossil fuels [4].

Renewable energy sources are significantly less harmful to the environment than conventional fossil fuel energy technologies [5]. These resources encompass solar, wind, geothermal, hydropower, and biomass energies [6]. Biomass is a renewable energy source with promising potential for different applications and can result in the production of power, heat, and biofuels [7]. Biomass is any organic material formed either directly or indirectly from photosynthesis. The sources of biomass include algae, aquatic crops, agricultural and forestry waste, animal manure, as well as municipal solid waste (MSW). Its biogenic origin makes it a renewable energy source since the carbon dioxide emitted during its combustion and exploitation does not cause a rise in the atmospheric carbon dioxide [8]. Bioenergy can be obtained through a variety of methods, such as thermochemical and biochemical methods [2]. Depending on the method, these conversion processes can produce solid char, liquid bio-oil, ethanol, biodiesel, syngas, or biogas [8].

Biodiesel, essentially a methyl ester, is one of the most well-known biofuels produced from biomass and can be utilized in conventional engines by blending it with regular diesel [9]. It is safer to store than petroleum due to its higher flash point [10]. Additionally, it can help mitigate the harmful impacts on the environment by decreasing carbon dioxide emissions [11]. The most prevalent biodiesel production method is the transesterification of oils or fats using alcohol and a catalyst [9]. However, the production process and yield obtained are greatly affected by several factors such as the availability and cost of the feedstock, type and quantity of catalyst used, alcohol-to-oil molar ratio, temperature of the reaction, reaction time, and stirring speed [12]. Therefore, optimizing these parameters can be beneficial in terms of enhancing resource utilization and yield, especially when producing large amounts of biodiesel.

RSM is a technique used to investigate the impact of a single independent variable or a group of variables on the dependent variable. Applying this mathematical model to the process of transesterification, this technique can be utilized to optimize operating conditions and maximize biodiesel production. As biodiesel yield can be predicted by simply adjusting the operational conditions, RSM can save time and money by reducing the need for a higher number of practical experiments. Using accurate error estimates, the model can mimic the reaction under different transesterification conditions [13]. RSM is a useful method to investigate how manipulating multiple parameters concurrently impacts the response [2]. RSM also includes a response surface, which aids in visualizing the results of the experimental study [14]. Some of the most frequently used designs are the Box-Behnken (BBD) and central composite designs (CCDs) [15]. The BBD lacks the extreme factor combinations or the vertices of the experimental cubic space, whereas the central composite explores borderline regions. As a result, BBD contains fewer experimental points and fewer degrees of freedom for the same number of parameters [16]. CCDs often anticipate more precise outcomes, and it is regarded as one of the most commonly utilized designs for second-order models [15]. In this study, the CCD was chosen since it can Energies 2025, 18, 4944 3 of 26

estimate the curvature in responses for a reasonable number of experiments. Several researchers have examined the application of RSM for the optimization of biodiesel production by optimizing parameters such as the methanol-to-oil ratio, catalyst loading, temperature, and time [17–22].

Different types of catalysts can be employed in biodiesel production, such as homogeneous, heterogeneous, and nanocatalysts [23]. Homogeneous catalysts are generally difficult to separate and recover; however, exceptionally active homogeneous catalysts may be left in the biodiesel product, since their residual concentration remains within acceptable impurity limits [24]. This limitation has nonetheless increased interest in the utilization of heterogeneous catalysts [25]. Heterogeneous catalysts have a few significant disadvantages, including the poisoning of the catalyst with exposure to air, sensitivity to free fatty acids and soap creation, and the possibility of contamination from the leaching of active sites [26]. Nanocatalysts can significantly increase the biodiesel production quality and yield while reducing reaction time [27]. Nano zeolites, oxides of metals, nano hydrotalcites, as well as magnetic nanocatalysts are examples of nanocatalysts that have demonstrated improved selectivity and yield. Combining two or more nanocatalysts improves productivity and simplifies purification, making heterogeneous nanocatalysts an excellent choice [28].

In this study, the biodiesel production process was carried out with the use of a blend of waste cooking oil and inedible neem oil catalyzed by a nanocatalyst that has not yet been explored for this application. The use of this feedstock blend is beneficial for the environment in terms of reducing waste as well as utilizing inedible oil. The neem tree has the ability to grow rapidly in severe conditions, and the neem oil obtained from this tree is an inedible oil with advantages such as reducing competition with food and land resources—a disadvantage of first-generation fuels produced from edible feedstock. Additionally, employing nanocatalysts in the process of biodiesel production has been shown to improve the obtained yield, reduce the time required, and allow for catalyst reusability in the case of heterogeneous nanocatalysts.

The process was optimized to maximize the biodiesel yield percentage using RSM by changing four independent variables: concentration of catalyst, duration, alcohol-to-oil molar ratio, and ratio of blend of oils. The study addresses the lack of understanding regarding the effectiveness of using a blend of waste cooking oil and inedible neem oil on the biodiesel yield and reaction parameters. It provides optimal solutions that can increase the efficiency and sustainability of biodiesel production, evaluate the effectiveness of a novel nanocatalyst in improving yields, as well as study its reusability and leaching of metals. The outcomes of this research contribute to the wider adoption of biodiesel as a sustainable fuel source by addressing economic and environmental concerns in biodiesel production.

2. Materials and Methods

2.1. Materials

The waste oil was collected from a local source that collects used cooking oil from several fast-food restaurants in Dubai and pretreated via filtering and drying to remove suspended impurities and eliminate residual moisture, ensuring a consistent quality of the feedstock despite the varying waste oil sources. The neem oil was commercially purchased online, and methanol (extrapure AR, 99.8%, SRL (Sisco Research Laboratories Pvt. Ltd., Mumbai, India) was used as the alcohol reagent. The catalyst used was a Cobalt Zinc Iron Oxide (CoZnFe₄O₈) nanopowder of 30–50 nm particle size, purchased from Nanostructured & Amorphous Materials, Inc. (NanoAmor, Los Alamos, NM, USA).

Energies 2025, 18, 4944 4 of 26

2.2. Characterization

The calorific value and density of the oils to be utilized for transesterification and the product biodiesel were measured using the Parr 6400 calorimeter and the portable density meter DA-130N. Fourier Transform Infrared (FTIR) analysis of the oils was carried out using the Jasco FTIR-6300 with ATR unit, and the spectra were recorded with a resolution of 2 cm⁻¹ and 16 scans in the range of 3600–400 cm⁻¹. The carbon, hydrogen, nitrogen, and sulfur contents in the biodiesel were measured using the vario MACRO cube elemental analyzer.

The nanocatalyst was characterized using X-Ray Diffraction (XRD), Brunauer–Emmett–Teller (BET) adsorption–desorption, X-ray Photoelectron Spectroscopy (XPS), Transmission Electron Microscopy (TEM), and thermogravimetric analysis (TGA) techniques. XRD pattern was measured using the BRUKER D8 ADVANCE (Bruker, Karlsruhe, Germany), and the BET surface area and pore size were measured using the NOVA TOUCH (Quantachrome Instruments, Boynton Beach, FL, USA). XPS analysis was carried out using the Nexsa G2 (Thermo Scientific, East Grinstead, UK) spectrometer using a monochromatized Al- $K\alpha$ radiation (1486.6 eV) under ultra-high vacuum (~10–9 mbar). Furthermore, TGA was performed using the Simultaneous Thermal Analyzer (Netzsch STA 449 F5) (Netzsch, Selb, Germany) in the range of 17.5 °C to 800 °C at a heating rate of 10 K/min under a nitrogen atmosphere.

2.3. Design of Experiments and Statistical Analysis

The design of experiments was conducted through RSM using Design Expert Software (Version 13.0). In this study, the input variables considered were the catalyst concentration, methanol-to-oil molar ratio, reaction duration, and waste cooking oil (WCO)-to-neem oil ratio (v/v), with biodiesel yield as the response. The levels for each variable and the ranges are shown in Table 1. Using the CCD, the Design Expert software designed 30 experimental runs. The Analysis of Variance (ANOVA) method was used to evaluate Fisher's test value (F-value), probability value (p-value), and coefficient of variation (p-value) to assess the effectiveness and significance of the RSM model.

Factor	Symbol	T T! £	Levels		
ractor		Unit	-1	0	1
Catalyst concentration	A	wt%	2	3.5	5
Methanol-to-oil molar ratio	В	-	6:1	13:1	20:1
Time	С	mins	60	150	240
WCO: Neem	D	-	0:100	50:50	100:0

Table 1. Four input variable levels for the CCD.

2.4. Experimental Procedure

The experimental setup for the transesterification reaction is provided in Supplementary Figure S1. First, the feedstock blend of waste cooking oil and neem oil was preheated to 65 °C, and the methanol and catalyst were added. For instance, for a run using a 3.5 wt% catalyst concentration, 13:1 methanol-to-oil molar ratio, 150 min, and a WCO/neem ratio of 50:50, the amount of catalyst, methanol, WCO, and neem oil used were 1.6 g, 30.9 mL, 25 mL, 25 mL, respectively. Next, the mixture was stirred for the desired reaction time. At the end of the reaction, the crude mixture is centrifuged to separate the biodiesel, glycerol, and catalyst. The biodiesel yield was then calculated using Equation (1). This gravimetric method has been consistently reported in the literature [29,30] as a practical approach for determining yield, and it also facilitates comparability with previous studies.

$$Yield (\%) = \frac{Mass \ of \ biodiesel}{Mass \ of \ feedstock \ oil}$$
 (1)

Energies 2025, 18, 4944 5 of 26

2.5. Catalyst Recovery and Reuse

The heterogeneous catalyst was recovered through centrifugation, washed with ethanol several times to remove adsorbed oil and glycerol residues, left to air-dry to remove residual ethanol, and then dried in an oven before reusing in subsequent reactions to evaluate its reusability.

3. Results and Discussion

This section demonstrates the results and analysis of the catalyst characterization—XRD, BET adsorption—desorption, XPS, TEM, and TGA—and feedstock properties—heating value, density, and FTIR. The experimental results and statistical analysis using RSM are discussed, including the model fit statistics and statistical plots, interactions of the parameters, and model optimization. Additionally, the biodiesel characterization results—heating value, density, FTIR, and ultimate analysis—are evaluated. Finally, the catalyst recovery, reusability, and leaching are discussed.

3.1. Catalyst Characterization

3.1.1. X-Ray Diffraction (XRD)

The XRD pattern of the heterogeneous Cobalt Zinc Iron Oxide (CoZnFe₄O₈) nanocatalyst is shown in Figure 1. The sharp peaks in the XRD pattern are consistent with a crystalline structure. The presence of magnetite (Fe₃O₄, PDF # 19-0629) [31] was detected at 20 values of around 30.96°, 35.41°, 43.07°, 57.08° and 62.49° [32], corresponding to the (220), (311), (400), (511), and (440) Miller indices [33]. In addition, several of the magnetite peaks can also be attributed to the zinc oxide wurtzite structure [34] (PDF # 36-1451) [35]. In addition to the peaks at 35.41°, 43.07°, 57.08°, and 62.49°, the peaks at 18.29°, 36.97°, and 53.37° corresponding to the (111), (222), and (422) planes can be assigned to cobalt oxide [36,37] (PDF# 42-1467) [38]. Previous studies have reported that enhanced crystallinity of the catalyst could potentially increase its stability and reusability compared to amorphous catalysts [39].

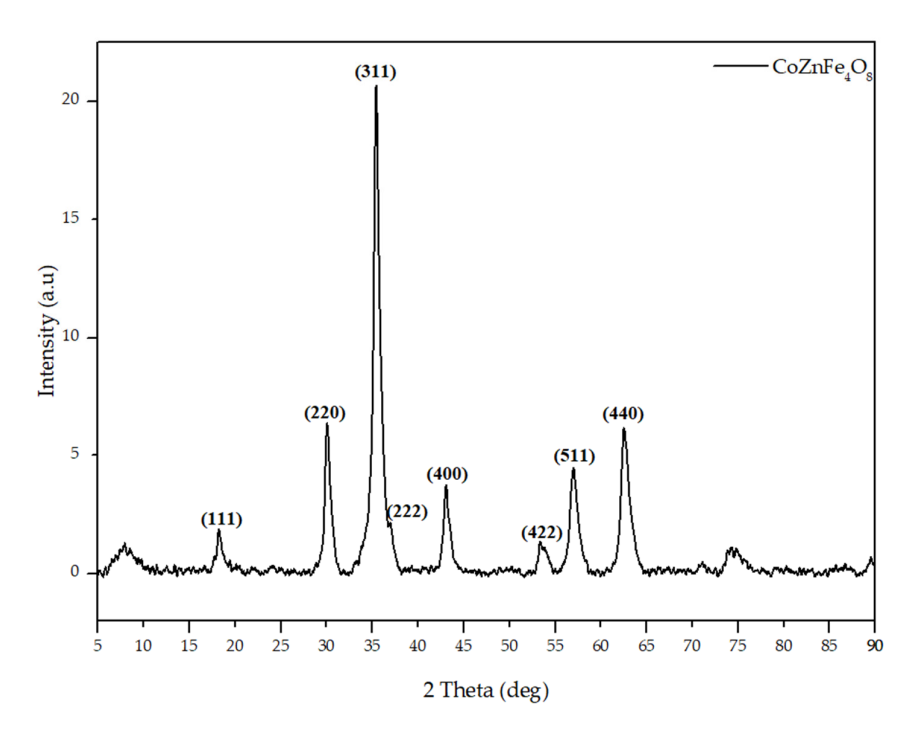


Figure 1. XRD pattern of the cobalt zinc iron oxide nanocatalyst used for the biodiesel production process.

Energies 2025, 18, 4944 6 of 26

3.1.2. Brunauer–Emmet–Teller (BET) Analysis

The BET method was employed to assess the surface area and pore characteristics of the catalyst, with results indicating a type IV isotherm (Figure 2), typical of mesoporous solids [40]. Variations in the amount of adsorbed gas during adsorption and desorption create a hysteresis loop [41]. The curves in Figure 2 correspond to a hysteresis loop Type H3 found in solids of plate-like particles aggregated with slit-like pores [40,42]. The average pore radius is 16.2 nm, and the BET surface area is 39.1 m²/g. The mesoporous nature of the catalyst and high BET surface can result in better catalytic activity [43]. Triglyceride molecules have an effective size of approximately 1.5–2.0 nm, which is smaller than the catalyst pore radius [44]. Catalysts of larger average pore diameters have been suggested to be effective in minimizing diffusion limitations for reactant molecules. This facilitates enhanced infiltration of reactants and ensures optimal utilization of active sites during the reaction [45].

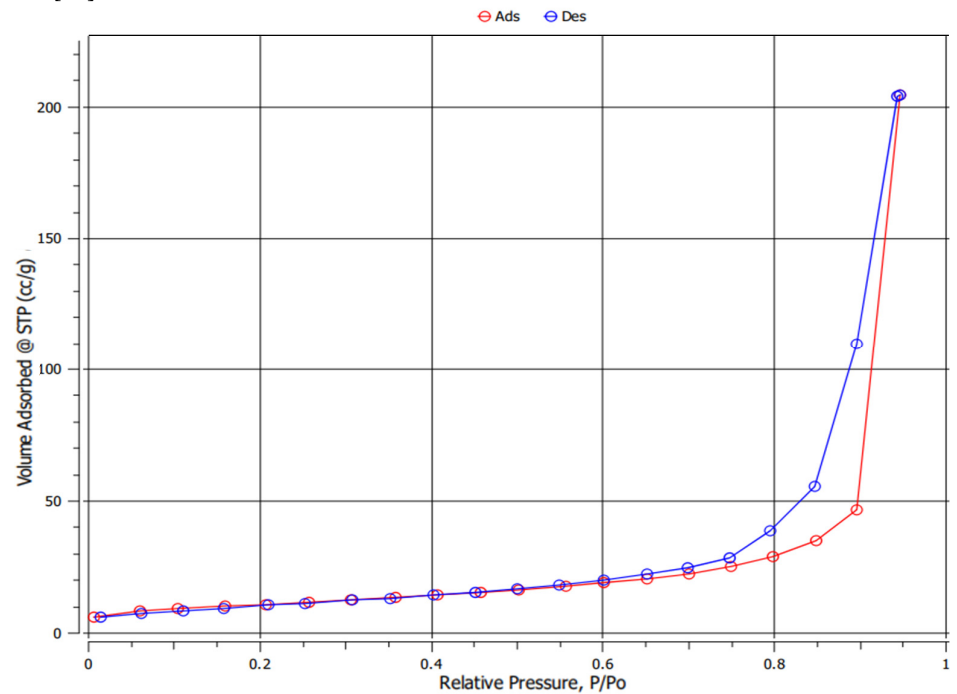


Figure 2. Brunauer–Emmet–Teller (BET) analysis for the nanocatalyst used in the biodiesel production experiment.

3.1.3. X-Ray Photoelectron Spectroscopy (XPS)

The XPS graph in Figure 3 demonstrates the presence of zinc, iron, cobalt, oxygen, carbon, and nitrogen elements in the heterogeneous nanocatalyst used. The higher counts per second for the zinc, iron, cobalt, and oxygen indicate higher concentrations of these elements in the sample, whereas the concentrations of nitrogen and carbon are significantly lower.

Energies 2025, 18, 4944 7 of 26

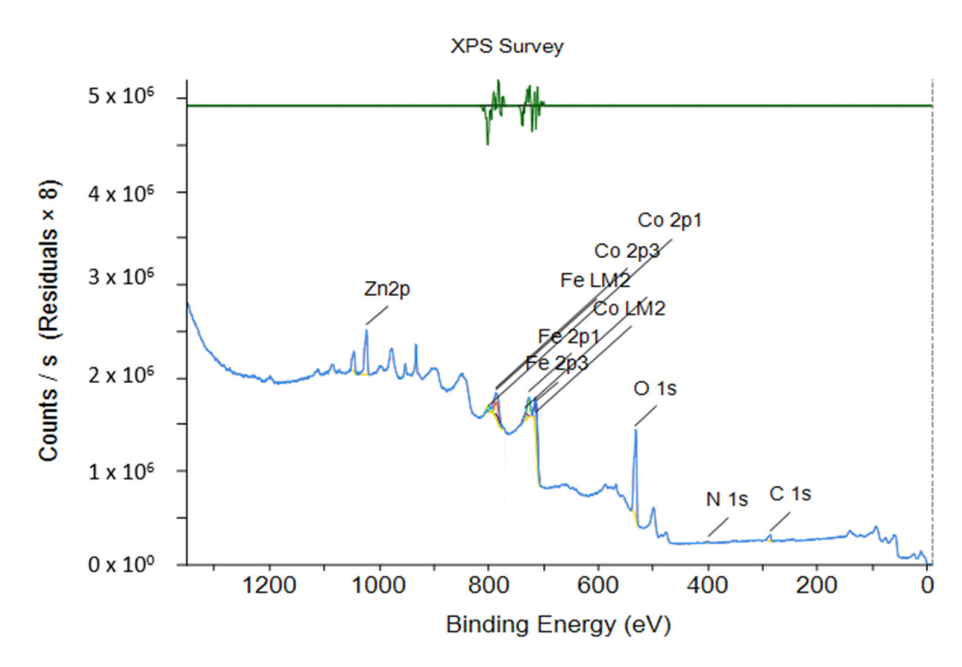


Figure 3. XPS spectrum of cobalt zinc iron oxide nanocatalyst.

3.1.4. Transmission Electron Microscopy (TEM)

The TEM micrograph of the heterogeneous nanocatalyst at a 100 nm scale is shown in Figure 4. The dark spots are individual nanoparticles or clusters of nanoparticles, and the varying intensity of darkness indicates differences in electron density or thickness, with darker regions corresponding to overlapping particles or denser particle domains. The figure reveals aggregated nanosized particles with predominant spherical morphology. The average particle size is approximately within the tens of nanometers range (~30 nm), consistent with the reported size distribution and literature reports of spinel ferrite nanoparticles, where CoFe₂O₄ particle sizes ranging from 3.5 nm to 80 nm have been observed depending on synthesis conditions [46]. The observed morphology supports the nanoscale structure and porosity characteristics inferred from the BET analysis.

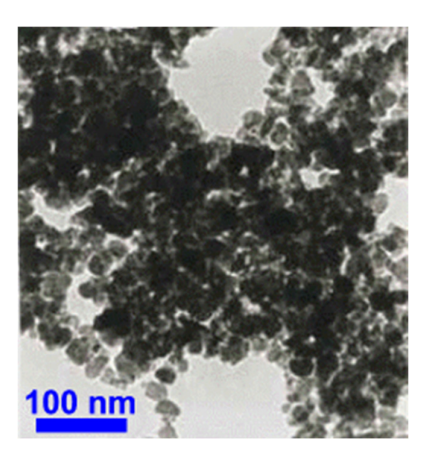


Figure 4. TEM image of nanocatalyst [47].

3.1.5. Thermogravimetric Analysis (TGA)

TGA was carried out on the nanocatalyst sample in the range of 17.5 °C to 800 °C at a heating rate of 10 °C/min under a nitrogen atmosphere. Figure 5 represents the mass percentage versus the temperature for the nanopowder sample. The first significant

Energies 2025, 18, 4944 8 of 26

decrease in Mass% occurs at approximately 103 °C and can be attributed to the drop in moisture content. The green curve in Figure 5 represents the derivative of mass loss and shows peaks that represent mass loss events during the stages of decomposition. The sharpest peak corresponds to the moisture content loss at around 100 °C, as is also apparent in the Mass%. Another smaller decomposition occurs at around 250 °C, which could be due to the decomposition of other volatile matter in the sample. The overall weight loss was around 11%.

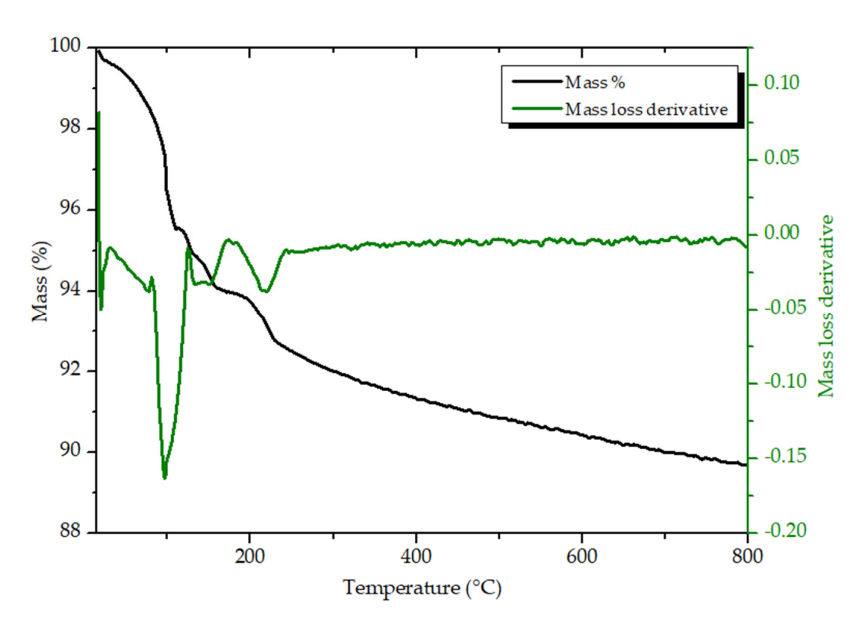


Figure 5. TGA of cobalt zinc iron oxide nanopowder.

3.2. Feedstock Characterization

The oil feedstocks were characterized using the higher heating value (HHV), density, and Fourier Transform Infrared (FTIR) analysis. The values of HHV for the feedstocks were very similar at 39.3 MJ/kg, 39.1 MJ/kg, and 39.6 MJ/kg, for waste cooking oil, neem oil, and the 50:50 blend, respectively. The measured density of the neem oil was 0.924 g/cm³, while the densities of the waste cooking oil and the blend were 0.916 g/cm³ and 0.912 g/cm³.

FTIR analysis of neem oil and WCO (Figure 6) was performed to compare the functional groups of the two feedstocks and highlight compositional differences that may influence biodiesel production. For neem oil, characteristic absorption bands were observed at 2920 cm⁻¹ and 2852 cm⁻¹ (C–H stretching), 1743 cm⁻¹ (C=O stretching of esters) [48], 1460 cm⁻¹ (C–H bending vibrations of CH₂/CH₃) [49], 1158 cm⁻¹ and 1029 cm⁻¹ (C–O stretching of esters) [49,50], and 723 cm⁻¹ (CH₂ rocking) [51]. The spectra of neem oil and WCO share similarities but also exhibit differences in band sharpness and intensity. In WCO, the ester-related bands appear weaker and less sharply defined compared to neem oil, which can be attributed to its mixed-source origin and compositional variability. These spectral variations suggest a partial alteration of triglyceride structures in WCO. The main peaks and their literature references are summarized in Table 2.

Energies 2025, 18, 4944 9 of 26

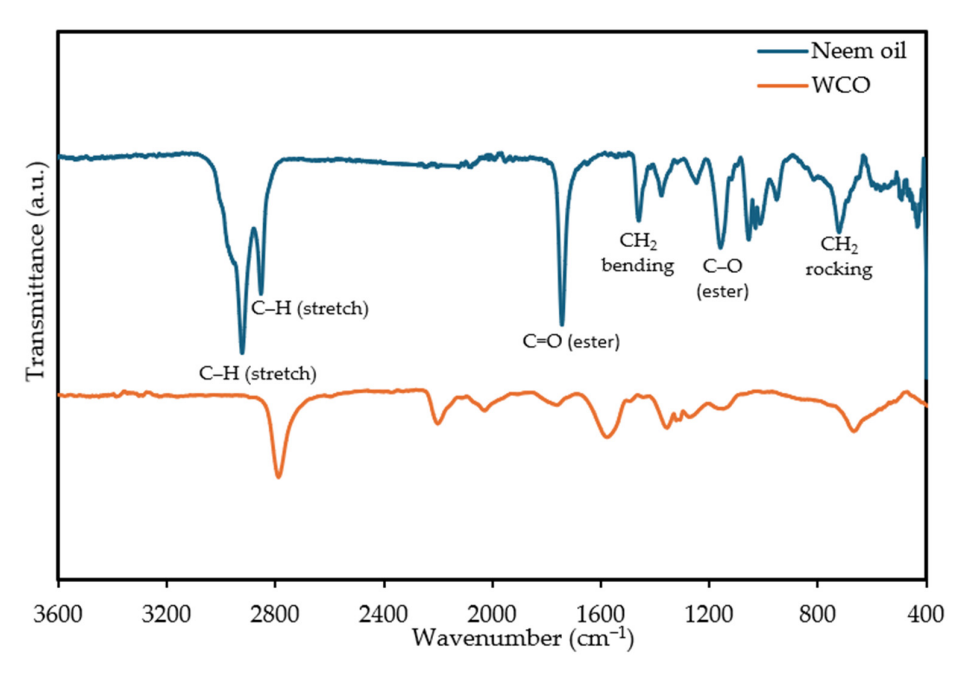


Figure 6. FTIR spectra of neem oil and waste cooking oil.

Table 2. FTIR peak assignments for neem oil and WCO.

Wavenumber (cm ⁻¹)	Assignment	Reference
2920, 2852	C-H stretching (CH ₂ , CH ₃)	[48]
1743	C=O stretching (ester)	[48,52]
1460	C-H bending (CH ₂ /CH ₃)	[49]
1158, 1029	C–O stretching (ester)	[49,50]
723	CH2 rocking	[51]

3.3. Statistical Analysis of Transesterification Experiments

Table 3 below presents the values of the input parameters considered for the transesterification experiments and the corresponding biodiesel yield obtained using the novel CoZnFe₄O₈ nanocatalyst. These yields are particularly significant as they demonstrate the catalyst's performance, providing crucial insights into its potential in biodiesel production. The total number of runs was 30, and the experimental runs were randomized in order.

 $\textbf{Table 3.} \ Experimental \ design \ and \ biodiesel \ yields \ using \ CoZnFe_4O_8 \ nanocatalyst.$

		Factor 1	Factor 2	Factor 3	Factor 4	Response
Std	Run	A:	В:	C:	D:	Biodiesel Yield
ota	Kuii	Catalyst Concentration	Methanol-to-oil	Time	WCO: Neem	(%)
		(wt%)	Molar Ratio	(Minutes)	wco: Neem	(/0)
10	1	5	6	60	100	89.8
6	2	5	6	240	0	90.64
14	3	5	6	240	100	87.61
25	4	3.5	13	150	50	86
12	5	5	20	60	100	90.43
22	6	3.5	13	240	50	90.98
4	7	5	20	60	0	86.35
21	8	3.5	13	60	50	91.23
17	9	2	13	150	50	90.07

Energies 2025, 18, 4944 10 of 26

24	10	3.5	13	150	100	91.77
2	11	5	6	60	0	90.49
26	12	3.5	13	150	50	89.02
1	13	2	6	60	0	89.95
9	14	2	6	60	100	93.71
7	15	2	20	240	0	86.05
30	16	3.5	13	150	50	86.73
3	17	2	20	60	0	80.42
27	18	3.5	13	150	50	88.76
18	19	5	13	150	50	92.71
28	20	3.5	13	150	50	87.83
13	21	2	6	240	100	94.1
5	22	2	6	240	0	90.61
20	23	3.5	20	150	50	87.14
19	24	3.5	6	150	50	90.48
29	25	3.5	13	150	50	86.38
8	26	5	20	240	0	83.07
11	27	2	20	60	100	89.24
16	28	5	20	240	100	82.63
15	29	2	20	240	100	93.36
23	30	3.5	13	150	0	87.13
			· ·	· ·	· ·	

The model fit summary is demonstrated in Table 4. p-values less than 0.05 suggest a significant model, and therefore, if the p-value > 0.5, a more complex model is needed to fit the data better [53]. The lack of fit p-value should be insignificant (>0.5) if the model is an adequate fit for the data, since a significant lack of fit implies variation in response around the fitted model [54]. The coefficient of determination (R^2) is a critical parameter that represents the square of the statistical variance between the experimental and model-calculated data. The closer the R^2 value is to 1, the better the fit the model is [55]. Adjusted R^2 is fine-tuned to the number of predictors in the regression equation, preventing the model from becoming overparameterized, and is often more conservative [56]. Based on these criteria, the suggested model by the software is the 2FI (two-factor interaction) with a low p-value, insignificant lack of fitness, and the highest R^2 values among the different models.

The standard deviation value and the coefficient of variation (CV) indicate the degree of precision [57]. The low CV of 2.28% implies that the data has minimal variability relative to the mean, indicating relatively consistent measurements. Furthermore, the R² value of 74.62% is considered a good value and indicates that the model fits the data well. A good R2 is dependent on the application; for instance, biological and social sciences are known for their high levels of noise and more weakly linked variables, and therefore a lower value is anticipated in these domains; a value of 0.6 may be regarded as good, and a value of 70% would already be regarded as high. However, in physics, a higher value is anticipated since the majority of data comes from well-regulated experiments [58]. The R² value of 74% in this study reflects a 26% variability attributed to experimental noise; nevertheless, the model performance is consistent with values reported for catalytic process models. To confirm the model's significance, the F-test is often used in addition to the R² [59]. The term "Adequate precision" is used to analyze the signal-to-noise ratio, which should be higher than 4 [60]. In this study, the ratio is 10.958, indicating that the model is reliable. In addition, the adjusted R² value of 0.6127 is lower than R² since it penalizes for non-significant terms. Based on the ANOVA in Table 5, factors A and C were statistically insignificant on their own but were retained in the model due to their significant interaction effects with other variables. Nevertheless, the model is statistically significant as Energies 2025, 18, 4944 11 of 26

indicated by the low p-value (0.0007) and an adequate precision ratio above 10. The predicted R^2 is considerably lower than both the R^2 and adjusted R^2 , which indicates a limited ability of the RSM to generalize well to unseen data.

Table 4. Model fit statistics.

Source	Sequential <i>p</i> - Value	Lack of Fit <i>p</i> - Value	\mathbb{R}^2	Adjusted R ²	
Linear	0.0040	0.0412	0.4471	0.3587	
2FI	0.0127	0.1097	0.7462	0.6127	Suggested
Quadratic	0.7244	0.0793	0.7770	0.5689	
Cubic	0.5916	0.0261	0.8869	0.5314	Aliased
Std. Dev.	2.03				
Mean	88.82				
C.V. %	2.28				
Adeq Precision	10.9576				
Adjusted R ²	0.6127				
Predicted R ²	0.2257				

To examine the RSM model's effectiveness and significance, the ANOVA approach was used to evaluate the F-value and *p*-value of the model and parameters. As seen in Table 5, the *p*-value for the model is 0.0007, which is lower than 0.05, making the model significant. In addition, the model terms B (Methanol-to-oil ratio), D (WCO/neem), AC, and AD are also significant. Greater F-values indicate greater significance of the terms on the response [61]. The model's F-value of 5.59 suggests the model is significant with just a 0.07% probability that it is due to noise. The overall lack of *p*-value fit is not significant, which suggests an adequate model fit. Even though factors A and C were not significant for this model, their interactions between AC and AD were significant, and the effects of the factors cannot be disregarded since they are theoretically important due to their combined effects on the response yield.

Table 5. ANOVA for 2FI model.

Source	Sum of Squares	Df	Mean Square	F-Value	<i>p</i> -Value	
Model	229.46	10	22.95	5.59	0.0007	significant
A-Catalyst concentration	10.55	1	10.55	2.57	0.1255	
B-Methanol-to-oil ratio	83.20	1	83.20	20.26	0.0002	
C-Time	0.3669	1	0.3669	0.0893	0.7683	
D-WCO/neem	43.37	1	43.37	10.56	0.0042	
AB	0.6561	1	0.6561	0.1598	0.6938	
AC	35.76	1	35.76	8.71	0.0082	
AD	34.40	1	34.40	8.38	0.0093	
ВС	0.0072	1	0.0072	0.0018	0.9670	
BD	16.48	1	16.48	4.01	0.0596	
CD	4.67	1	4.67	1.14	0.2998	
Residual	78.03	19	4.11			
Lack of Fit	69.94	14	5.00	3.09	0.1097	not significant
Pure Error	8.09	5	1.62			
Cor Total	307.49	29				

Energies 2025, 18, 4944 12 of 26

The final model equation (Equation (2)) to predict the biodiesel yield is as below:

Biodiesel yield = 85.84948 + 1.87753 * A - 0.514583 * B + 0.043611 * C + 0.079769 * D + 0.019286 * AB - 0.011074 * AC - 0.019550 * AD - 0.000034 * BC + 0.002900 (2) * BD - 0.000120 * CD

Figure 7a shows the normal plot of residuals, where all the points fall roughly along the straight line. A normal plot of residuals with no noticeable deviations from the line suggests that the residuals are mostly normally distributed, and the model can be considered adequate. The graph of residuals vs. predicted values (Figure 7b) shows a random distribution of the residual points and no clear pattern in the plot, which implies constant variance and no reason to suspect dependency. The colored points in the plots represent the range of the biodiesel yield, where blue and red represent the lowest and highest yields, respectively.

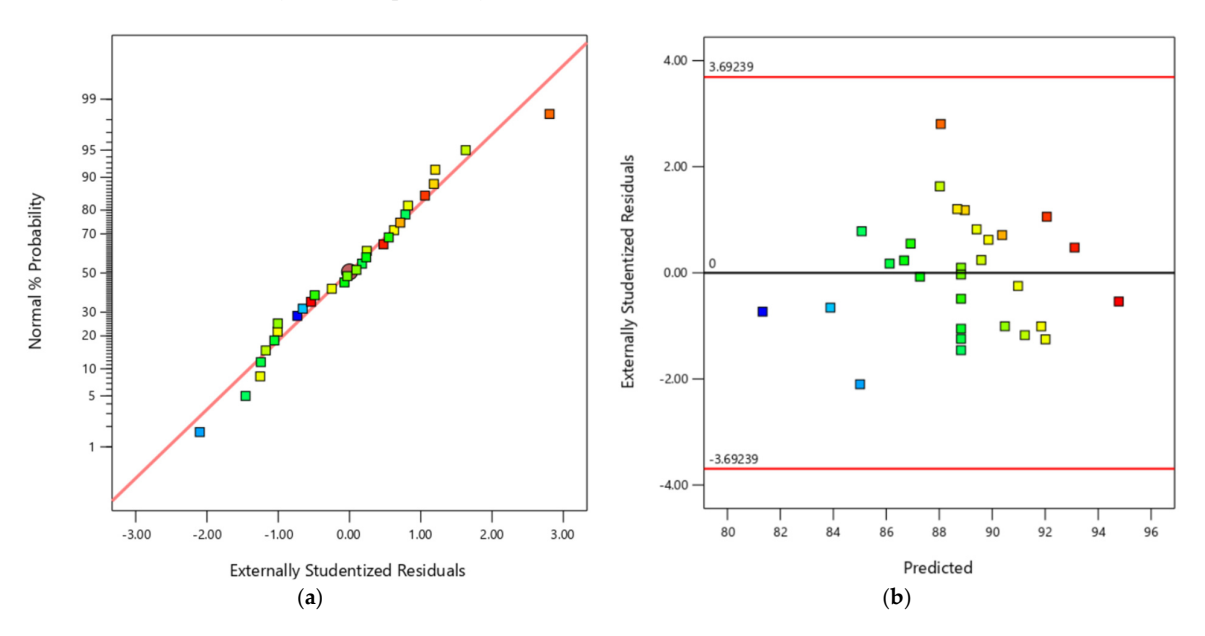


Figure 7. (a) Normal plot of residuals; and (b) R = residuals vs. predicted values plot. Point colors represent biodiesel yield, with blue indicating the lowest and red indicating the highest yields.

Figure 8a–d show the residuals plotted against each of the four independent variables. All the plots exhibit a random scatter of residuals across (no clear trend in the spread), indicating that the variance in biodiesel yield is constant regardless of the independent variables. There are no outliers, and the absence of patterns or trends in the residuals supports the model's reliability.

Energies 2025, 18, 4944 13 of 26

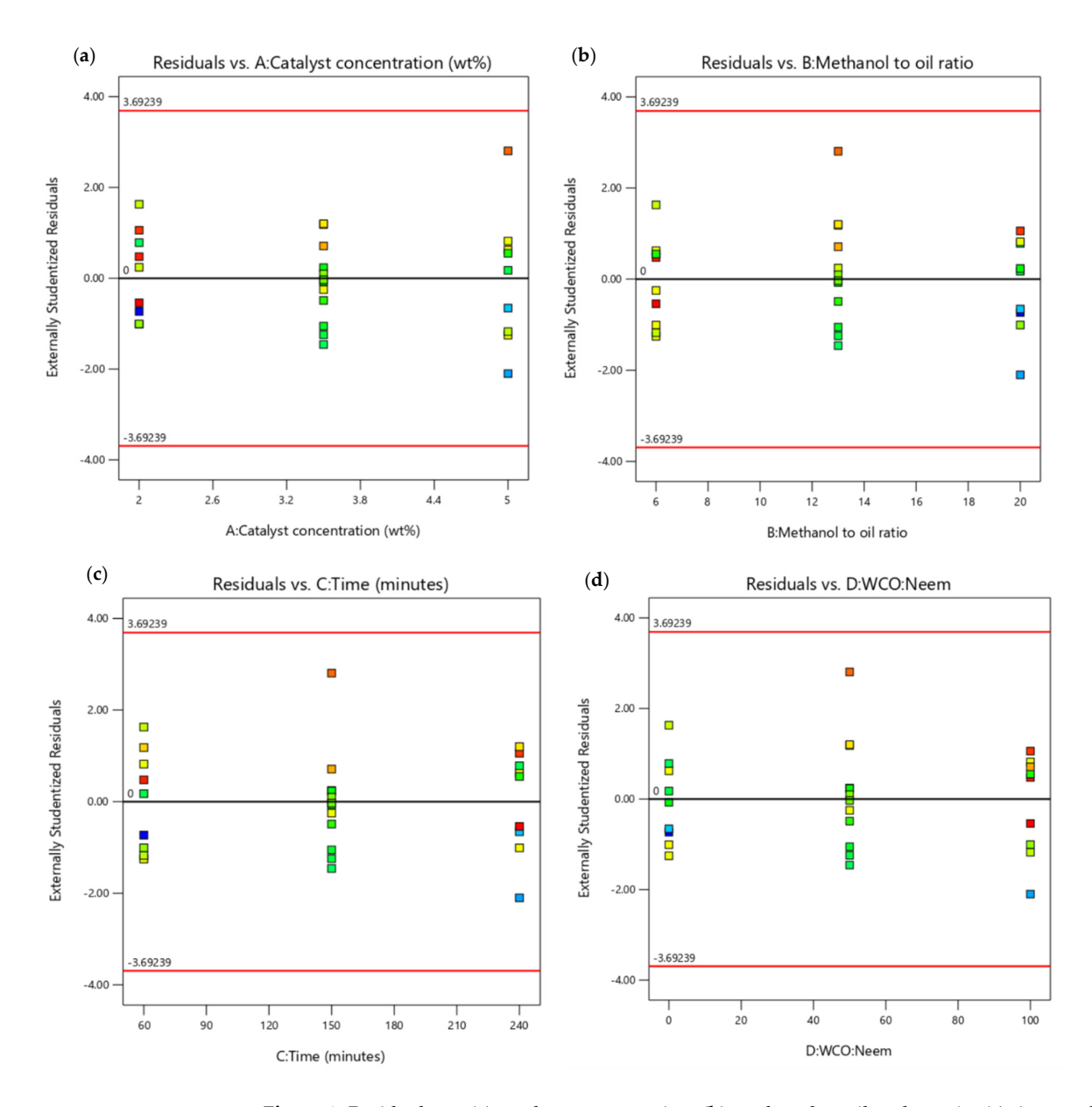


Figure 8. Residuals vs. (a) catalyst concentration; (b) methanol-to-oil molar ratio; (c) time; and (d) WCO to neem. Point colors represent biodiesel yield, as described in Figure 7.

The predicted vs. actual yield graph in Figure 9 demonstrates that the model is a good fit for the prediction of the response (i.e., biodiesel yield) since there is close correspondence between the predicted and actual values. A few points show a difference between the actual and predicted yields, which may be attributed to experimental variability or unaccounted interactions in the model.

Energies 2025, 18, 4944 14 of 26

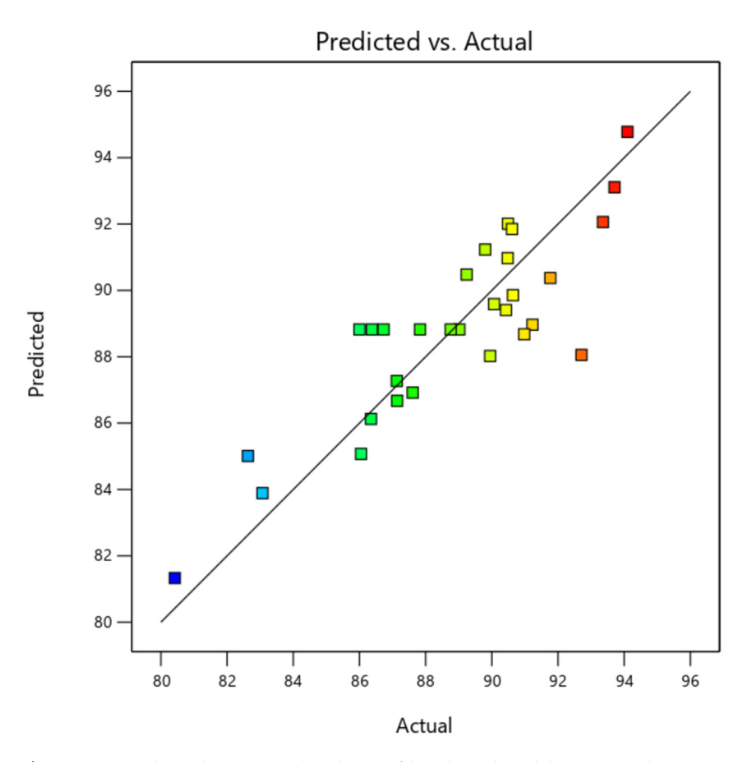


Figure 9. Predicted vs. actual values of biodiesel yield. Point colors represent biodiesel yield, as described in Figure 7.

3.4. Parameter Interactions and 3-D Plots

Figure 10a-f show the 3-D response surface plots for the interaction of the independent variables and the biodiesel yield. In Figure 10a, the combined interaction of catalyst concentration and methanol-to-oil molar ratio on the yield is shown. The highest predicted yield appears to be in the lower range of the catalyst concentration and at higher methanol-to-oil ratios. The interaction between the catalyst concentration and time (Figure 10b) demonstrates that the catalyst concentration does not have a significant impact on this interaction, whereas longer reaction times at lower catalyst concentration increase the yield. The curve in Figure 10c indicates that the effect of the catalyst concentration varies with the WCO/neem ratio, supporting the significant AD interaction term. As evidenced by the relatively flat response surface in Figure 10d, the interaction between the methanol-to-oil ratio and reaction time on the yield has minimal effect. Furthermore, the plot of the methanol-to-oil ratio and WCO/neem vs. the biodiesel yield (Figure 10e) shows that lower methanol-to-oil ratios and higher WCO ratios result in better yield. Finally, the lack of significant curvature in Figure 10f indicates that time does not significantly interact with the WCO/neem ratio, which is also proven by the ANOVA results. Overall, the effect of time on the yield in the interactions considered was not very significant, whereas the methanol-to-oil and waste cooking oil to neem oil ratios seem to have a larger impact on the response.

Energies 2025, 18, 4944 15 of 26

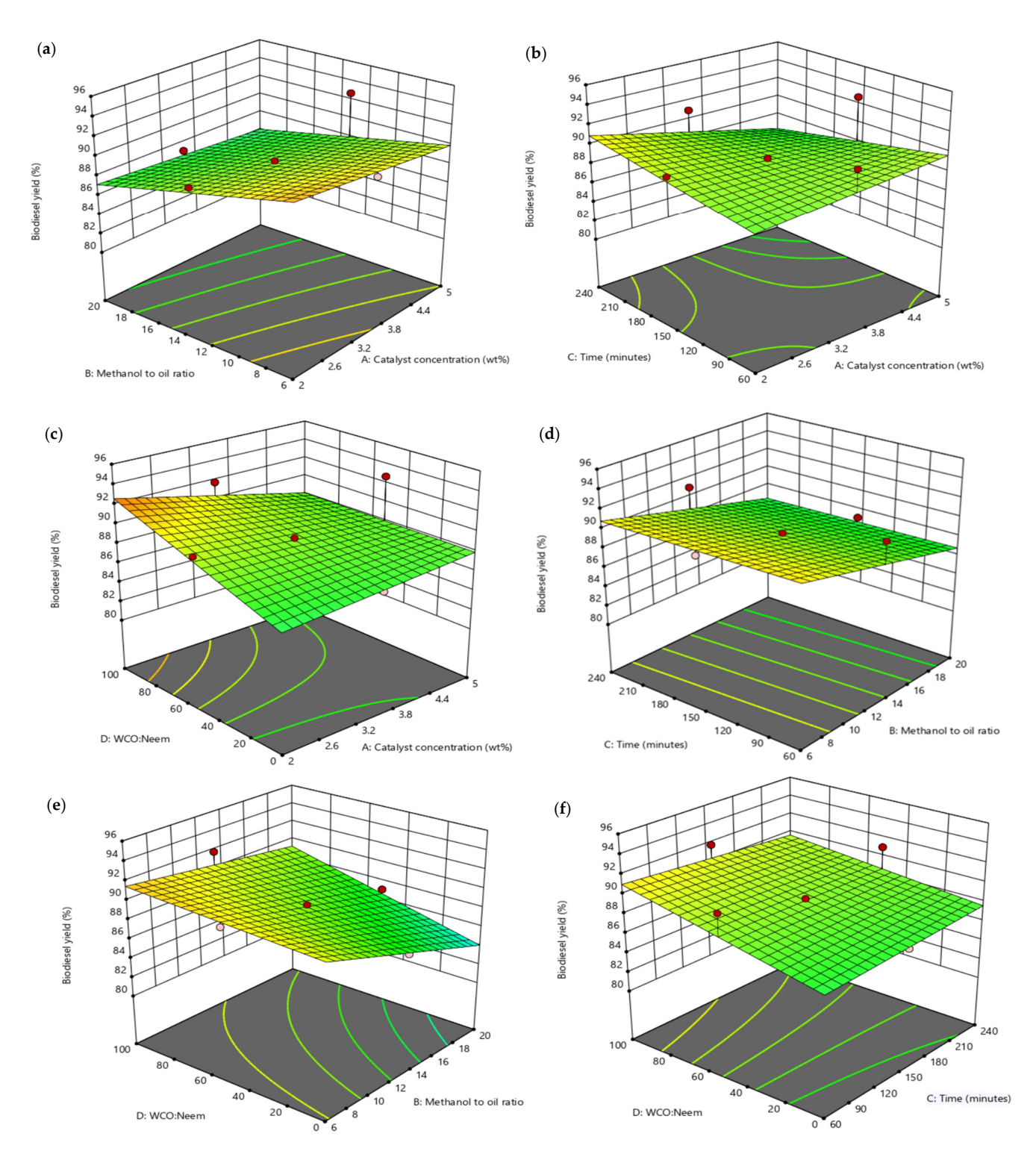


Figure 10. Three-dimensional surface plots for interaction between response and the following: (a) catalyst concentration and methanol-to-oil molar ratio; (b) catalyst concentration and time; (c) catalyst concentration and WCO/neem; (d) methanol-to-oil ratio and time; (e) methanol-to-oil ratio and WCO/neem; and (f) time and WCO/neem. Surface colors indicate the predicted biodiesel yield from lower to higher values (green to yellow/orange).

To further illustrate the significant interactions between AC and AD, the 2-D contours in Figure 11 can be examined. In the 2D plots, the contour lines represent the levels of biodiesel yield, and the change in color of the plot from green to orange represents an

Energies 2025, 18, 4944 16 of 26

increasing yield percentage. As seen in the first plot (Figure 11a) and the 3-D plot in Figure 10b, lower catalyst concentrations and higher reaction time can increase the yield. The areas with no contour lines are ranges where the change in catalyst concentration or time has little effect on yield. The interaction of the catalyst concentration and WCO/neem ratio has a considerable impact on the yield, as seen in Figure 11b. This effect could be due to a higher catalyst affinity in terms of conversion of triglycerides in the case of WCO compared to neem.

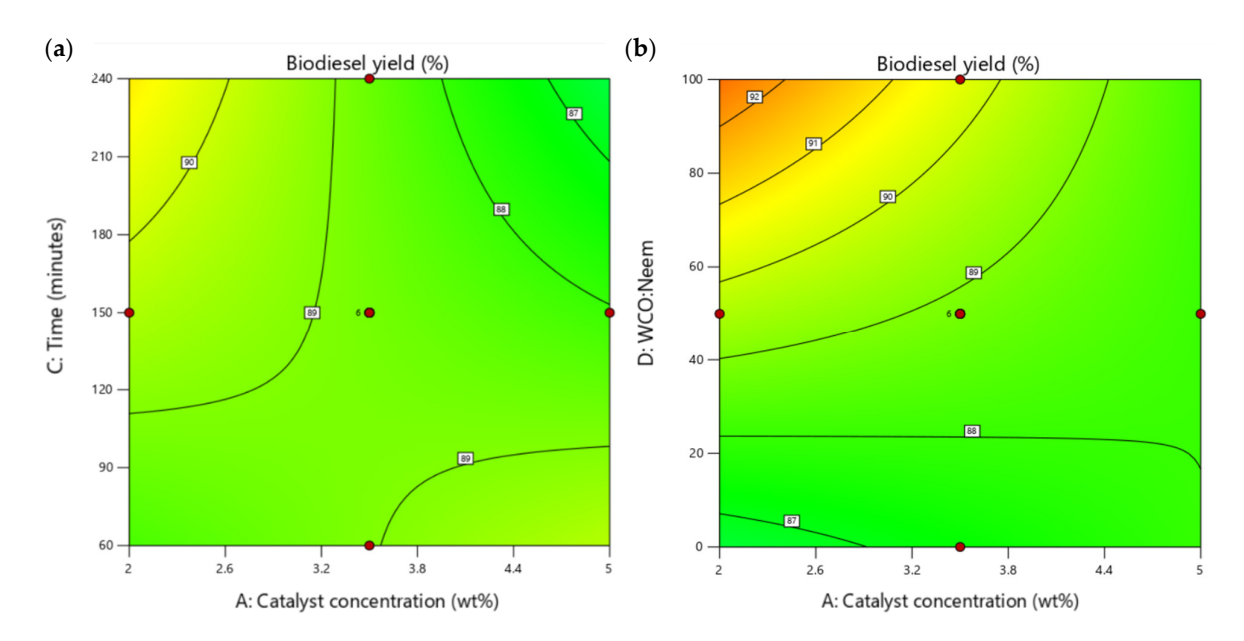


Figure 11. Two-dimensional contour plots for interactions of the following: (a) catalyst concentration and time; and (b) catalyst concentration and WCO/neem ratio. Surface colors represent biodiesel yield, as described in Figure 10.

The perturbation graph in Figure 12 shows the impact of each of the four factors on the response. Based on the graph, the two steeper slopes are the lines associated with factors B and D, which indicate that these two factors have the most effect on the yield. Factor B has a negative impact on the yield, while factor D has a positive impact. On the other hand, changes in factors A and C do not have as much influence as indicated by the lower slopes, which also supports the earlier demonstrations from the surface plots and ANOVA results that indicated minimal impact of catalyst concentration and reaction time.

Energies 2025, 18, 4944 17 of 26

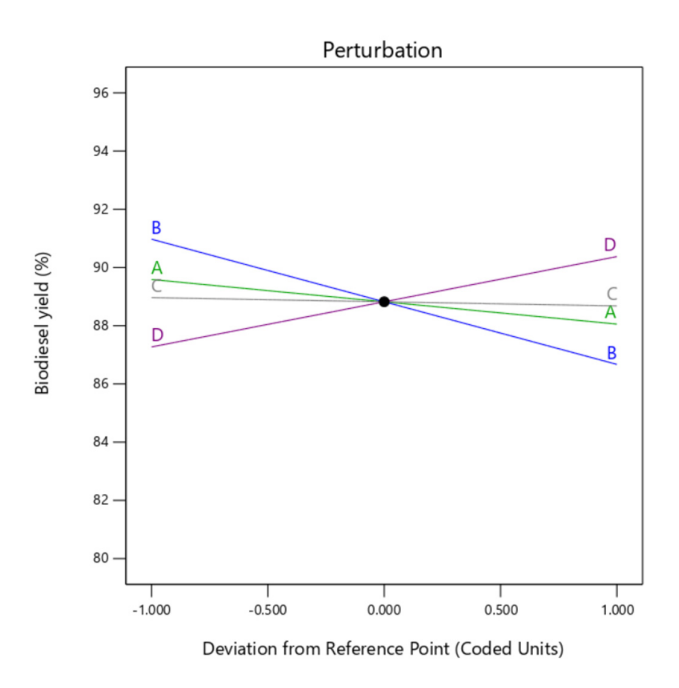


Figure 12. Perturbation plots.

3.5. Model Optimization

The optimum catalyst amount, methanol-to-oil molar ratio, time, and ratio of waste cooking oil to neem oil were found to be 2.13 wt%, 6.80:1, 4 h, and 98.32:1.68, respectively, as shown in Figure 13. These optimum conditions would result in a 94.23% predicted biodiesel yield. These results are close to the experimental results obtained of a 94.10% yield using 2 wt% catalyst, 6:1 methanol-to-oil ratio, 4 h, and a 100:1 waste cooking oil-to-neem oil ratio.

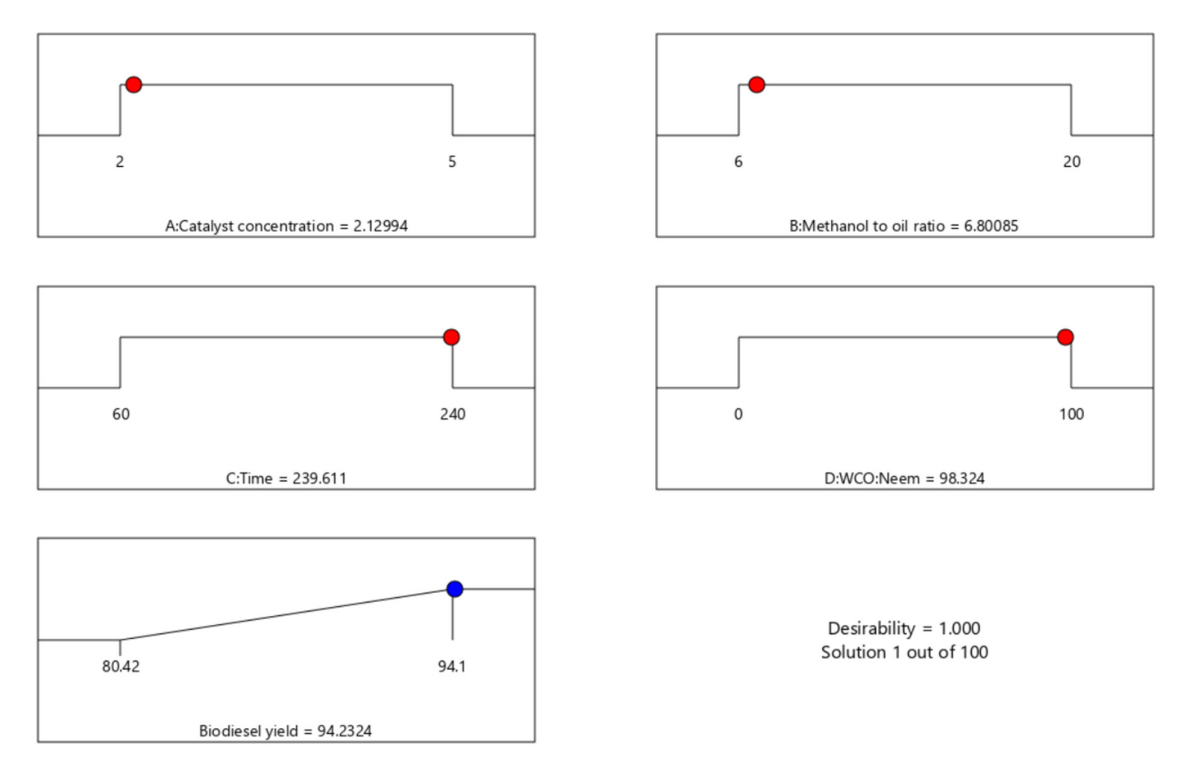


Figure 13. Optimized parameters.

Energies 2025, 18, 4944 18 of 26

3.6. Catalyst Performance Comparison

The performance of the novel CoZnFe₄O₈ nanocatalyst was compared to other heterogeneous nanocatalysts, homogeneous base catalysts, homogeneous acid catalysts, and enzyme catalysts reported in the literature in order to assess its efficiency in the biodiesel production application. Table 6 shows the catalyst used, feedstock, reaction conditions, and biodiesel yield for several heterogeneous nanocatalysts used in previous studies. The yield obtained from the present study (94.10%) utilizing the CoZnFe₄O₈ nanocatalyst is comparable to yields obtained from reported studies utilizing different heterogeneous, homogeneous, and enzyme catalysts. These findings indicate the potential of the CoZnFe₄O₈ nanocatalyst for efficient biodiesel production under optimal reaction circumstances.

Table 6. Performance comparison of CoZnFe₄O₈ nanocatalyst and other catalysts for biodiesel production.

Catalyst	- 0.5 - 7.5 Waste frying oil ratio - 30		Reaction Conditions	Biodiesel Yield	Reference
NaOH			0.5 wt% catalyst 7.5:1 methanol-to-oil molar 30 min 50 °C	96%	[62]
ZnO/BiFeO3 magnetic nanocata- lyst	Canola oil	- - ratio	4 wt% catalyst 15:1 methanol-to-oil molar 6 h	95.43%	[63]
CaO/CuFe2O4 nanoparticles	Chicken fat	- - -	3% catalyst loading 15:1 methanol-to-oil ratio 4 h 70°C	94.52%	[64]
CoZnFe₄Os nanopowder	Waste cooking oil and neem oil		2 wt% catalyst loading6:1 anol-to-oil molar ratio 4 h 100:1 WCO-to-neem oil ra- 65 °C	94.10%	Present study
MgO nanocatalyst	Goat fat	- ratio -	1 wt% catalyst 12:1 methanol-to-oil molar 3 h 70 °C	93.12%	[65]
TiO2 nanoparticles	Waste cooking/frying olive oil	- g ratio - -	30:1 methanol-to-oil molar 4 h 120 °C	91.2%	[66]
H ₂ SO ₄	Waste cooking oil	- ratio -	4 wt% catalyst 20:1 methanol-to-oil molar 40 min 95 °C	90%	[67]
Lipase	Waste cooking oil	- ratio -	1.5 wt% catalyst 3:1 methanol-to-oil molar 4 h 65 °C	88%	[68]

Energies 2025, 18, 4944 19 of 26

3.7. Biodiesel Characterization

The biodiesel sample used to measure the heating value and density, as well as for the FTIR analysis, was obtained from the optimum biodiesel run based on the RSM and experimental findings.

3.7.1. Heating Value

The higher heating value of the biodiesel was found to be 38.2 MJ/kg. Although the American Society for Testing and Materials (ASTM) D6751 standards [69] do not specify ranges of heating value [70], it is prescribed in EN 14213 [71] (biodiesel for heating purposes) with a minimum of 35 MJ/kg [72]. The measured heating value is within standard ranges of biodiesel heating values.

3.7.2. Density

The density of the produced biodiesel was measured at standard conditions of $20 \,^{\circ}$ C and 1 atm. The measured density of $0.9137 \, \text{g/cm}^3$ is close to the normal ranges reported in the literature of $0.825-0.931 \, \text{g/cm}^3$ [73].

3.7.3. FTIR

Figure 14 shows the spectra of biodiesel against WCO in order to compare the biodiesel to the feedstock that was used in the optimum run (WCO), as well as to confirm the conversion into methyl ester. The two plots have similar peaks at around 2786 cm⁻¹, 2201 cm⁻¹, and 2023 cm⁻¹. There are more differences in the region between 1500 cm⁻¹ and 800 cm⁻¹, including the peak in the biodiesel spectra at 1444 cm⁻¹, suggesting substantial –CH₂ stretching, which contributes to greater carbon content [74]. The peaks at around 1735 cm⁻¹, 1580 cm⁻¹, and 670 cm⁻¹ are more intense in the biodiesel plot. The peak at 1735 cm⁻¹ is sharper and more intense due to the C=O vibration representative of the carbonyl ester bond [75].

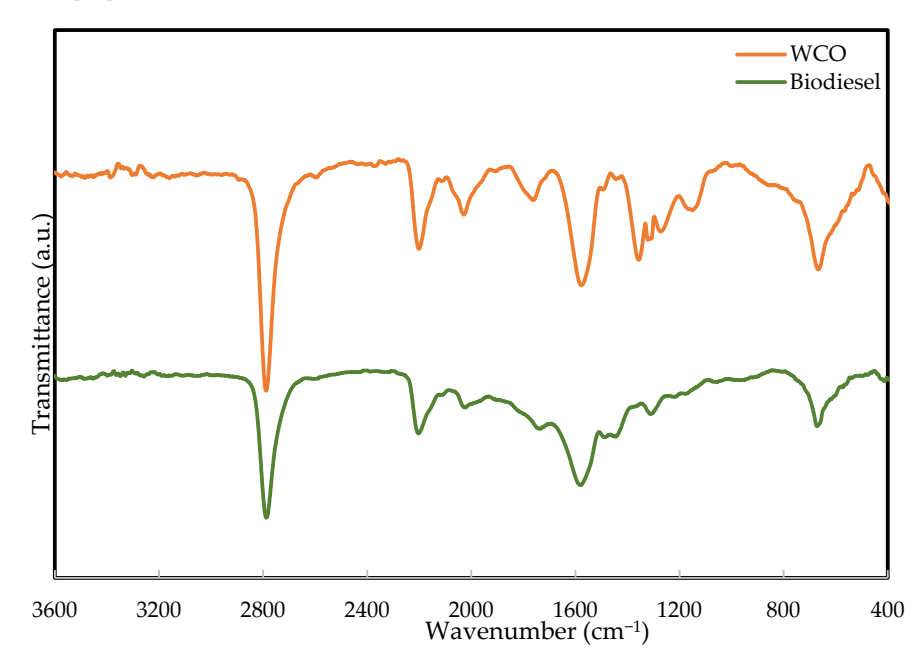


Figure 14. FTIR spectra of biodiesel vs. WCO.

Energies 2025, 18, 4944 20 of 26

3.7.4. Ultimate Analysis

The ultimate analysis of the biodiesel produced was carried out to obtain the percentages of carbon, hydrogen, nitrogen, and sulfur. The carbon, hydrogen, nitrogen, and sulfur contents in the biodiesel were 69.89%, 4.76%, 0.05%, and 0.0063%, respectively. According to the ASTM-D6751 standard, sulfur content should be less than 0.05 wt% [72], which is the case with the produced biodiesel. The sulfur level of a fuel affects engine wear and deposits. It is damaging to both human health and the environment [76], and hence it is important for the sulfur content in biodiesel to be low. In addition, lower sulfur and nitrogen contents in the fuel result in lower SO_x and NO_x emissions [74]. Carbon and hydrogen contents are the primary factors for the quality of fuel and are responsible for the increased calorific value [74]. The percentages of carbon and hydrogen in the sample are within the range of reported percentages for biodiesel [74,77]. A summary of the measured biodiesel properties compared to reference ranges in the literature is presented in Table 7.

Table 7. Properties of produced biodiesel.

Property	Measured Value (This Study)	Range	Reference
HHV (MJ/kg)	38.15	>35	[72]
Density at 20 °C (g/cm ³)	0.9137	0.825-0.931 a	[73]
Carbon (%)	69.89	~60–80	[74,77]
Hydrogen (%)	4.76	~11–12.6	[74,77]
Nitrogen (%)	0.05	0.03	[74]
Sulfur (%)	0.0063	0.05	[72]

^a Values vary with temperature and source of feedstock.

3.8. Catalyst Reusability

After catalyst recovery, the reused catalyst from run 10 (Supplementary Figure S2) was tested in a subsequent experiment. The catalyst recovered after the first reuse was further tested in a second reuse experiment. The reuse experiments were carried out using 3.5 wt% catalyst, 13:1 methanol-to-oil molar ratio, 150 min reaction time, and 100:0 WCO/neem oil ratio. The yields obtained from the reuse experiments are demonstrated in Figure 15, which shows that the heterogeneous nanocatalyst is reusable but with some decrease in efficiency. The results represent a 10.51% decrease in yield after the first reuse, and an additional 1.51% decrease in yield from the first reuse to the second. The loss in the catalytic activity could be attributed to the decrease in the BET surface area of the catalyst [78] or the leaching of the metals in the catalyst.

Energies 2025, 18, 4944 21 of 26

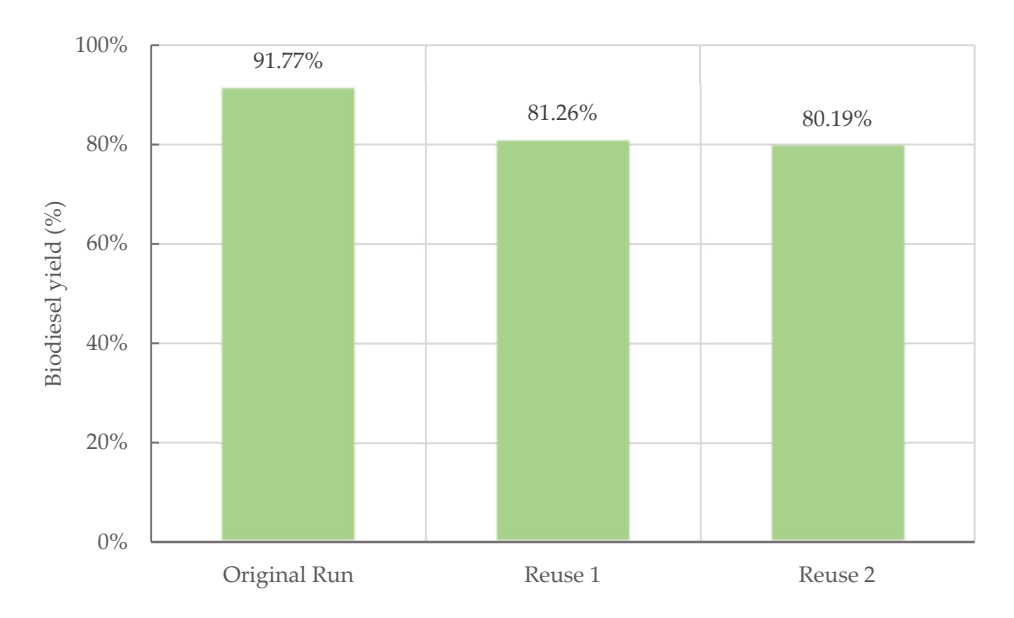


Figure 15. Yield of biodiesel using recovered catalyst.

3.9. Metal Leaching from the CoZnFe₄O₈ Catalyst

Inductively Coupled Plasma-Optical Emission Spectrometry (ICP-OES) analysis was conducted to assess the leaching of the metals (Co, Zn, Fe) from the CoZnFe₄O₈ catalyst into biodiesel. As seen in Table 8, the concentrations of cobalt and zinc in the biodiesel samples were higher compared to the feed oils, confirming that these metals leached from the catalyst during the transesterification process. On the other hand, iron concentrations remained somewhat constant, suggesting higher structural stability of Fe compared to Co and Zn within the catalyst lattice. The leaching of active metals from the catalyst can reduce its catalytic activity and reusability, as well as complicate post-reaction separation and purification of the biodiesel product. Previous studies have highlighted that heterogeneous catalyst deactivation is often linked to leaching, ultimately limiting their reusability; however, supported catalysts are generally more resistant to leaching and can retain their activity over longer reusability cycles [79]. Additionally, feedstock acidity is known to influence yield [80], and in some cases (e.g., MgO), FFA presence may accelerate catalyst leaching through Mg soap formation [81].

Table 8. ICP-OES results for Co, Zn, and Fe concentrations (mg/L) in feedstock oils and the corresponding biodiesel product.

Sample	Co (mg/L)	Fe (mg/L)	Zn (mg/L)
Neem oil	0.1458	4.2028	0.1077
Biodiesel (Neem oil)	0.5115	4.0455	1.0976
WCO	0.2709	4.5458	0.0587
Biodiesel (WCO)	0.4751	4.0323	0.2536

4. Conclusions

The process of biodiesel production with the use of a sustainable blend of waste cooking oil and neem oil and a novel heterogeneous nanocatalyst was carried out and then optimized using RSM alongside a CCD. The ANOVA was used to investigate the significance of the developed model using statistical measures such as the p-value, coefficient of variation (R^2), and lack of fit tests. According to the statistical analysis, the low p-value (p < 0.05) with a robust F-value, R^2 of 74.62%, and the insignificant lack of fit suggested the

Energies 2025, 18, 4944 22 of 26

model is adequate and reliable. The significant model terms were the methanol-to-oil molar ratio, WCO/neem ratio, as well as the interactions of the catalyst concentration with time and the catalyst concentration with WCO/neem ratio. Furthermore, the actual biodiesel yields obtained experimentally closely matched the predicted yields, confirming the model's ability to accurately predict the response. The normal probability plot indicated the model was adequate and there were no significant deviations from normality, and the residual plots showed no clear trends in the residual points, indicating constant variance and the reliability of the model. The optimal combination of factors was found to be a catalyst concentration of 2.13 wt%, a methanol-to-oil ratio of 6.80:1, a reaction duration of 4 h, and a waste cooking oil to neem oil ratio of 98.32:1.68, under which the achieved biodiesel yield is 94.23%. These results closely correspond with the achieved experimental yield of a 94.10% yield using 2 wt% catalyst, 6:1 methanol-to-oil molar ratio, 240 min reaction time, and 100:1 waste cooking oil to neem oil ratio. In addition, the reusability of the cobalt zinc iron oxide (CoZnFe₄O₈) nanocatalyst was assessed by recovering the catalyst and reusing it. This analysis showed a 10.51% reduction in biodiesel yield after the first reuse, and a further 1.51% decrease in yield in the second reuse, which could be attributed to a decrease in the BET surface area or leaching of the cobalt and zinc metals from the catalyst.

The study also provided a thorough characterization of the nanocatalyst, feedstock, and produced biodiesel. The catalyst characterization using XRD revealed a highly crystalline structure, and the BET analysis confirmed a mesoporous structure with a surface area of 39.145 m²/g, indicating high availability of catalytic sites for the transesterification reaction. The biodiesel heating value and density were within the normal range for biodiesel fuel, and the FTIR spectroscopy confirmed the successful transesterification of the feedstock oils into biodiesel, as evidenced by the difference in peaks and intensities. Ultimate analysis of the biodiesel showed good carbon and hydrogen contents and low sulfur and nitrogen levels, which is beneficial for reducing fuel emissions.

Therefore, the combination of the blend of waste and inedible oils and the novel nanocatalyst in biodiesel production showed promising potential for environmentally friendly biofuel production with an optimum yield greater than 94%. The novel nanocatalyst demonstrated great catalytic activity and offered the potential for reusability, a crucial aspect of sustainable biodiesel production. Moreover, the results of this study contribute to the ongoing efforts to achieve economically feasible and environmentally friendly biofuels.

Supplementary Materials: The following supporting information can be downloaded at: https://www.mdpi.com/article/10.3390/en18184944/s1. Figure S1: Experimental setup for the transesterification process of waste cooking oil and neem oil. Figure S2: Recovered CoZnFe₄O₈ catalyst after the transesterification reaction.

Author Contributions: Conceptualization, S.M.A. and A.I.; methodology, S.M.A. and A.I.; formal analysis, S.M.A.; investigation, S.M.A.; resources, A.I.; writing—original draft preparation, S.M.A.; writing—review and editing, S.M.A., A.I., F.J. and P.H.; visualization, S.M.A.; supervision, A.I., F.J. and P.H.; project administration, A.I.; funding acquisition, P.H. All authors have read and agreed to the published version of the manuscript. All authors have read and agreed to the published version of the manuscript.

Funding: This research received no external funding.

Data Availability Statement: The original contributions presented in this study are included in the article/Supplementary Material. Further inquiries can be directed at the corresponding authors.

Conflicts of Interest: The authors declare no conflicts of interest.

Energies 2025, 18, 4944 23 of 26

Abbreviations

The following abbreviations are used in this manuscript:

BBD Box-Behnken Design
BET Brunauer-Emmett-Teller
CCD Central Composite Design
FTIR Fourier Transform Infrared

ICP-OES Inductively Coupled Plasma-Optical Emission Spectrometry

RSM Response Surface Methodology

WCO Waste Cooking Oil XRD X-Ray Diffraction

References

1. Jones, C.S.; Mayfield, S.P. Our Energy Future: Introduction to Renewable Energy and Biofuels; University of California Press: Oakland, CA, USA, 2016. Available online: https://books.google.ae/books?id=K7QwDwAAQBAJ (accessed on 29 March 2023).

- 2. Asaad, S.M.; Inayat, A.; Rocha-Meneses, L.; Jamil, F.; Ghenai, C.; Shanableh, A. Prospective of Response Surface Methodology as an Optimization Tool for Biomass Gasification Process. *Energies* **2022**, *16*, 40. https://doi.org/10.3390/en16010040.
- 3. Mitchell, R.; Sweeney, F. *Air Pollution*; Scientific e-Resources: New Delhi, India, 2018. Available online: https://books.google.ca/books?id=WNW_DwAAQBAJ (accessed on 29 August 2025).
- 4. Soeder, D.J. Fossil Fuels and Climate Change. In *Fracking and the Environment*; Springer International Publishing: Cham, Switzerland, 2021. pp. 155–185. https://doi.org/10.1007/978-3-030-59121-2_9.
- 5. Shahzad, U. The need for renewable energy sources. Int. J. Inf. Technol. Electr. Eng. 2012, 2, 16–18.
- Qazi, A.; Hussain, F.; Rahim, N.A.B.D.; Hardaker, G.; Alghazzawi, D.; Shaban, K.; Haruna, K. Towards Sustainable Energy: A
 Systematic Review of Renewable Energy Sources, Technologies, and Public Opinions. *IEEE Access* 2019, 7, 63837–63851.
 https://doi.org/10.1109/ACCESS.2019.2906402.
- 7. Dahiya, A. *Bioenergy: Biomass to Biofuels and Waste to Energy*, 2nd ed.; Elsevier Inc.: Amsterdam, The Netherlands, 2020. Available online: https://www.sciencedirect.com/book/9780128154977/bioenergy (accessed on 18 November 2021).
- 8. Tursi, A. A review on biomass: Importance, chemistry, classification, and conversion. *Biofuel Res. J.* **2019**, *6*, 962–979. https://doi.org/10.18331/BRJ2019.6.2.3.
- Capareda, S. Introduction to Biomass Energy Conversions; CRC Press, Taylor & Francis Group: Boca Raton, FL, USA, 2013. https://doi.org/10.1201/b15089.
- 10. Russo, D.; Portarapillo, M.; Di Benedetto, A. Flash point of biodiesel/glycerol/alcohol mixtures for safe processing and storage. J. Loss Prev. Process Ind. 2023, 83, 105077. https://doi.org/10.1016/j.jlp.2023.105077.
- 11. Dincer, K. Lower Emissions from Biodiesel Combustion. *Energy Sources Part A Recover. Util. Environ. Eff.* **2008**, *30*, 963–968. https://doi.org/10.1080/15567030601082753.
- 12. Chozhavendhan, S.; Vijay Pradhap Singh, M.; Fransila, B.; Praveen Kumar, R.; Karthiga Devi, G. A review on influencing parameters of biodiesel production and purification processes. *Curr. Res. Green Sustain. Chem.* **2020**, 1–2, 1–6. https://doi.org/10.1016/j.crgsc.2020.04.002.
- 13. Dharma, S.; Masjuki, H.H.; Ong, H.C.; Sebayang, A.H.; Silitonga, A.S.; Kusumo, F.; Mahlia, T.M.I. Optimization of biodiesel production process for mixed Jatropha curcas-Ceiba pentandra biodiesel using response surface methodology. *Energy Convers. Manag.* 2016, 115, 178–190. https://doi.org/10.1016/j.enconman.2016.02.034.
- 14. Chen, W.-H.; Carrera Uribe, M.; Kwon, E.E.; Lin, K.-Y.A.; Park, Y.-K.; Ding, L.; Saw, L.H. A comprehensive review of thermoelectric generation optimization by statistical approach: Taguchi method, analysis of variance (ANOVA), and response surface methodology (RSM). *Renew. Sustain. Energy Rev.* 2022, 169, 112917. https://doi.org/10.1016/j.rser.2022.112917.
- 15. Asaad, S.M.; Inayat, A.; Ghenai, C.; Shanableh, A. Response Surface Methodology in Biodiesel Production and Engine Performance Assessment. *Int. J. Thermofluids* **2024**, *21*, 100551. https://doi.org/10.1016/j.ijft.2023.100551.
- Veljković, V.B.; Veličković, A.V.; Avramović, J.M.; Stamenković, O.S. Modeling of biodiesel production: Performance comparison of Box–Behnken, face central composite and full factorial design. *Chinese J. Chem. Eng.* 2019, 27, 1690–1698. https://doi.org/10.1016/j.cjche.2018.08.002.
- 17. Ayoub, M.; Ullah, S.; Inayat, A.; Bhat, A.H.; Hailegiorgis, S.M. Process Optimization for Biodiesel Production from Waste Frying Oil over Montmorillonite Clay K-30. *Procedia Eng.* **2016**, *148*, 742–749. https://doi.org/10.1016/j.proeng.2016.06.606.

Energies 2025, 18, 4944 24 of 26

18. Asaad, S.M.; Inayat, A.; Jamil, F.; Ghenai, C.; Shanableh, A. Optimization of Biodiesel Production from Waste Cooking Oil Using a Green Catalyst Prepared from Glass Waste and Animal Bones. *Energies* **2023**, *16*, 2322. https://doi.org/10.3390/en16052322.

- 19. Singh Pali, H.; Sharma, A.; Kumar, N.; Singh, Y. Biodiesel yield and properties optimization from Kusum oil by RSM. Fuel 2021, 291, 120218. https://doi.org/10.1016/j.fuel.2021.120218.
- 20. Bharti, P.; Singh, B.; Dey, R.K. Process optimization of biodiesel production catalyzed by CaO nanocatalyst using response surface methodology. *J. Nanostructure Chem.* **2019**, *9*, 269–280. https://doi.org/10.1007/s40097-019-00317-w.
- 21. Hasni, K.; Ilham, Z.; Dharma, S.; Varman, M. Optimization of biodiesel production from Brucea javanica seeds oil as novel non-edible feedstock using response surface methodology. *Energy Convers. Manag.* **2017**, 149, 392–400. https://doi.org/10.1016/j.enconman.2017.07.037.
- 22. Borah, M.J.; Das, A.; Das, V.; Bhuyan, N.; Deka, D. Transesterification of waste cooking oil for biodiesel production catalyzed by Zn substituted waste egg shell derived CaO nanocatalyst. *Fuel* **2019**, 242, 345–354. https://doi.org/10.1016/j.fuel.2019.01.060.
- 23. Hosseini, S.A. Nanocatalysts for biodiesel production. *Arab. J. Chem.* **2022**, *15*, 104152. https://doi.org/10.1016/j.arabjc.2022.104152.
- 24. Melchiorre, M.; Amoresano, A.; Budzelaar, P.H.M.; Cucciolito, M.E.; Mocerino, F.; Pinto, G.; Ruffo, F.; Tuzi, A.; Esposito, R. Parts-Per-Million (Salen)Fe(III) Homogeneous Catalysts for the Production of Biodiesel from Waste Cooking Oils. *Catal. Lett.* **2022**, *152*, 3785–3794. https://doi.org/10.1007/s10562-022-03948-x.
- 25. Ramos, M.; Dias, A.P.S.; Puna, J.F.; Gomes, J.; Bordado, J.C. Biodiesel production processes and sustainable raw materials. *Energies* **2019**, *12*, 4408. https://doi.org/10.3390/en12234408.
- 26. Okechukwu, O.D.; Joseph, E.; Nonso, U.C.; Kenechi, N.-O. Improving heterogeneous catalysis for biodiesel production process. *Clean. Chem. Eng.* **2022**, *3*, 100038. https://doi.org/10.1016/j.clce.2022.100038.
- 27. Bano, S.; Ganie, A.S.; Sultana, S.; Sabir, S.; Khan, M.Z. Fabrication and Optimization of Nanocatalyst for Biodiesel Production: An Overview. *Front. Energy Res.* **2020**, *8*, 579014. https://doi.org/10.3389/fenrg.2020.579014.
- 28. Asaad, S.M.; Inayat, A.; Jamil, F.; Ghenai, C.; Shanableh, A. Prospective of Nanocatalysts in Transesterification Process for the Biodiesel Production. In Proceedings of the 2023 Advances in Science and Engineering Technology International Conferences (ASET), Dubai, United Arab Emirates, 20–23 February 2023; pp. 1–5. https://doi.org/10.1109/ASET56582.2023.10180499.
- 29. Shah, M.; Ali, S.; Tariq, M.; Khalid, N.; Ahmad, F.; Khan, M.A. Catalytic conversion of jojoba oil into biodiesel by organotin catalysts, spectroscopic and chromatographic characterization. *Fuel* **2014**, *118*, 392–397. https://doi.org/10.1016/j.fuel.2013.11.010.
- 30. Mohamad, M.; Ngadi, N.; Wong, S.L.; Jusoh, M.; Yahya, N.Y. Prediction of biodiesel yield during transesterification process using response surface methodology. *Fuel* **2017**, *190*, 104–112. https://doi.org/10.1016/j.fuel.2016.10.123.
- 31. Aleman-Ramirez, J.L.; Reyes-Vallejo, O.; Okoye, P.U.; Sanchez-Albores, R.; Maldonado-Álvarez, A.; Sebastian, P.J. Crystal phase evolution of high temperature annealed Fe3O4-CaO catalysts for biodiesel production. *Biofuels Bioprod. Biorefining* **2023**, *17*, 843–858. https://doi.org/10.1002/bbb.2478.
- 32. Kumar, M.; Sharma, A.; Maurya, I.K.; Thakur, A.; Kumar, S. Synthesis of ultra small iron oxide and doped iron oxide nanostructures and their antimicrobial activities. *J. Taibah Univ. Sci.* **2019**, *13*, 280–285. https://doi.org/10.1080/16583655.2019.1565437.
- Macías-Martínez, B.I.; Cortés-Hernández, D.A.; Zugasti-Cruz, A.; Cruz-Ortíz, B.R.; Múzquiz-Ramos, E.M. Heating ability and hemolysis test of magnetite nanoparticles obtained by a simple co-precipitation method. *J. Appl. Res. Technol.* 2016, 14, 239–244. https://doi.org/10.1016/j.jart.2016.05.007.
- 34. Kumar, H.; Rani, R. Structural and Optical Characterization of ZnO Nanoparticles Synthesized by Microemulsion Route. *Int. Lett. Chem. Phys. Astron.* **2013**, *19*, 26–36. https://doi.org/10.56431/p-q38442.
- 35. Pasupulety, N.; Rempel, G.L.; Ng, F.T.T. Studies on Mg-Zn mixed oxide catalyst for biodiesel production. *Appl. Catal. A Gen.* **2015**, 489, 77–85. https://doi.org/10.1016/j.apcata.2014.10.015.
- Gul, I.; Khan, S.M.; Mehmood, T.; Ahmad, Z.; Badshah, H.; Shah, H. Characterization of Cobalt Oxide and Calcium-Aluminum Oxide nano-catalyst through Scanning Electron Microscopy, X-ray diffraction, and Energy Dispersive X-ray Spectroscopy. Microsc. Res. Tech. 2020, 83, 1124–1131. https://doi.org/10.1002/jemt.23504.
- 37. Lendzion-Bielun, Z.; Narkiewicz, U.; Arabczyk, W. Cobalt-based Catalysts for Ammonia Decomposition. *Materials* **2013**, *6*, 2400–2409. https://doi.org/10.3390/ma6062400.
- 38. Wang, S.; Zhang, X.; Huang, J.; Chen, J. High-performance non-enzymatic catalysts based on 3D hierarchical hollow porous Co3O4 nanododecahedras in situ decorated on carbon nanotubes for glucose detection and biofuel cell application. *Anal. Bioanal. Chem.* **2018**, 410, 2019–2029. https://doi.org/10.1007/s00216-018-0875-3.

Energies 2025, 18, 4944 25 of 26

39. Tong, D.-G.; Chu, W.; Luo, Y.-Y.; Ji, X.-Y.; He, Y. Effect of crystallinity on the catalytic performance of amorphous Co–B particles prepared from cobalt nitrate and potassium borohydride in the cinnamaldehyde hydrogenation. *J. Mol. Catal. A Chem.* **2007**, 265, 195–204. https://doi.org/10.1016/j.molcata.2006.10.032.

- 40. Yurdakal, S.; Garlisi, C.; Özcan, L.; Bellardita, M.; Palmisano, G. (Photo)catalyst Characterization Techniques. In *Heterogeneous Photocatalysis*; Elsevier: Amsterdam, The Netherlands, 2019, pp. 87–152. https://doi.org/10.1016/B978-0-444-64015-4.00004-3
- 41. Tompsett, G.A.; Krogh, L.; Griffin, D.W.; Conner, W.C. Hysteresis and Scanning Behavior of Mesoporous Molecular Sieves. *Langmuir* 2005, 21, 8214–8225. https://doi.org/10.1021/la050068y.
- 42. Bardestani, R.; Patience, G.S.; Kaliaguine, S. Experimental methods in chemical engineering: Specific surface area and pore size distribution measurements—BET, BJH, and DFT. *Can. J. Chem. Eng.* **2019**, *97*, 2781–2791. https://doi.org/10.1002/cjce.23632.
- 43. Changmai, B.; Sudarsanam, P.; Rokhum, S.L. Biodiesel production using a renewable mesoporous solid catalyst. *Ind. Crops Prod.* **2020**, *145*, 111911. https://doi.org/10.1016/j.indcrop.2019.111911.
- 44. List, G.R. Bleaching and Purifying Fats and Oils: Theory and Practice; Elsevier Inc.: Amsterdam, The Netherlands, 2009.
- 45. Lani, N.S.; Ngadi, N.; Yahya, N.Y.; Rahman, R.A. Synthesis, characterization and performance of silica impregnated calcium oxide as heterogeneous catalyst in biodiesel production. *J. Clean. Prod.* **2017**, 146, 116–124. https://doi.org/10.1016/j.jclepro.2016.06.058.
- 46. Mohapatra, J.; Xing, M.; Elkins, J.; Beatty, J.; Liu, J.P. Size-dependent magnetic hardening in CoFe 2 O 4 nanoparticles: Effects of surface spin canting. *J. Phys. D. Appl. Phys.* **2020**, *53*, 504004. https://doi.org/10.1088/1361-6463/abb622.
- 47. Nanostructured & Amorphous Materials, Inc. Cobalt-Zinc Iron Oxide Nanopowder (Co0.5Zn0.5Fe2O4, 99.5%, 30–50 nm). Available online: https://www.nanoamor.com/inc/sdetail/10983/3966 (accessed on 14 October 2024).
- 48. Li, H.; Niu, S.; Lu, C.; Wang, Y. Comprehensive Investigation of the Thermal Degradation Characteristics of Biodiesel and Its Feedstock Oil through TGA–FTIR. *Energy Fuels* **2015**, *29*, 5145–5153. https://doi.org/10.1021/acs.energyfuels.5b01054.
- 49. Samanta, S.; Sahoo, R.R. Waste Cooking (Palm) Oil as an Economical Source of Biodiesel Production for Alternative Green Fuel and Efficient Lubricant. *BioEnergy Res.* **2021**, *14*, 163–174. https://doi.org/10.1007/s12155-020-10162-3.
- 50. Abdullah; Rahmawati Sianipar, R.N.; Ariyani, D.; Nata, I.F. Conversion of palm oil sludge to biodiesel using alum and KOH as catalysts. *Sustain. Environ. Res.* **2017**, 27, 291–295. https://doi.org/10.1016/j.serj.2017.07.002.
- 51. Mekonnen, K.D. Fourier transform infrared spectroscopy as a tool for identifying the unique characteristic bands of lipid in oilseed components: Confirmed via Ethiopian indigenous desert date fruit. *Heliyon* **2023**, 9, e14699. https://doi.org/10.1016/j.heliyon.2023.e14699.
- 52. De, B.; Gupta, K.; Mandal, M.; Karak, N. Tough hyperbranched epoxy/neem-oil-modified OMMT thermosetting nanocomposite with an antimicrobial attribute. *N. J. Chem.* **2015**, *39*, 595–603. https://doi.org/10.1039/C4NJ01558D.
- 53. Muhammad, G.; Potchamyou Ngatcha, A.D.; Lv, Y.; Xiong, W.; El-Badry, Y.A.; Asmatulu, E.; Xu, J.; Alam, M.A. Enhanced biodiesel production from wet microalgae biomass optimized via response surface methodology and artificial neural network. *Renew. Energy* 2022, 184, 753–764. https://doi.org/10.1016/j.renene.2021.11.091.
- 54. Massoudinejad, M.; Sadani, M.; Gholami, Z.; Rahmati, Z.; Javaheri, M.; Keramati, H.; Sarafraz, M.; Avazpour, M.; Shiri, S. Optimization and modeling of photocatalytic degradation of Direct Blue 71 from contaminated water by TiO2 nanoparticles: Response surface methodology approach (RSM). *Iran. J. Catal.* **2019**, *9*, 121–132. Available online: https://oiccpress.com/jjc/article/view/4038 (accessed on 22 March 2024).
- 55. Peng, Y.; Khaled, U.; Al-Rashed, A.A.A.A.; Meer, R.; Goodarzi, M.; Sarafraz, M.M. Potential application of Response Surface Methodology (RSM) for the prediction and optimization of thermal conductivity of aqueous CuO (II) nanofluid: A statistical approach and experimental validation. *Phys. A Stat. Mech. Its Appl.* 2020, 554, 124353. https://doi.org/10.1016/j.physa.2020.124353.
- 56. Plonsky, L.; Ghanbar, H. Multiple Regression in L2 Research: A Methodological Synthesis and Guide to Interpreting R 2 Values. *Mod. Lang. J.* 2018, 102, 713–731. https://doi.org/10.1111/modl.12509.
- 57. Rewatkar, K.; Shende, D.Z.; Wasewar, K.L. Modeling and Optimization of Reactive Extraction of Gallic Acid Using RSM. *Chem. Eng. Commun.* **2017**, 204, 522–528. https://doi.org/10.1080/00986445.2017.1282470.
- 58. Faraway, J.J. *Practical Regression and ANOVA Using R*; Self-published; University of Michigan, MI, USA, 2002. Available online: http://csyue.nccu.edu.tw/Practical%20Regression%20and%20Anova%20using%20R.pdf (accessed on 18 May 2024).
- 59. Brown, S.; Tauler, R.; Walczak, B. (Eds.) *Comprehensive Chemometrics*; Elsevier: Amsterdam, The Netherlands, 2020. Available online: https://www.sciencedirect.com/referencework/9780444641663/comprehensive-chemometrics (accessed on 18 May 2024).
- 60. Prajapati, N.; Oza, S.; Kodgire, P.; Singh Kachhwaha, S. Microwave assisted biodiesel production: Assessment of optimization via RSM techniques. *Mater. Today Proc.* **2022**, *57*, 1637–1644. https://doi.org/10.1016/j.matpr.2021.12.243.

Energies 2025, 18, 4944 26 of 26

61. Onu, C.E.; Nwabanne, J.T.; Ohale, P.E.; Asadu, C.O. Comparative analysis of RSM, ANN and ANFIS and the mechanistic modeling in eriochrome black-T dye adsorption using modified clay. S. Afr. J. Chem. Eng. 2021, 36, 24–42. https://doi.org/10.1016/j.sajce.2020.12.003.

- 62. Uzun, B.B.; Kılıç, M.; Özbay, N.; Pütün, A.E.; Pütün, E. Biodiesel production from waste frying oils: Optimization of reaction parameters and determination of fuel properties. *Energy* **2012**, *44*, 347–351. https://doi.org/10.1016/j.energy.2012.06.024.
- 63. Salimi, Z.; Hosseini, S.A. Study and optimization of conditions of biodiesel production from edible oils using ZnO/BiFeO3 nano magnetic catalyst. *Fuel* **2019**, 239, 1204–1212. https://doi.org/10.1016/j.fuel.2018.11.125.
- 64. Seffati, K.; Honarvar, B.; Esmaeili, H.; Esfandiari, N. Enhanced biodiesel production from chicken fat using CaO/CuFe2O4 nanocatalyst and its combination with diesel to improve fuel properties. *Fuel* **2019**, 235, 1238–1244. https://doi.org/10.1016/j.fuel.2018.08.118.
- 65. Rasouli, H.; Esmaeili, H. Characterization of MgO nanocatalyst to produce biodiesel from goat fat using transesterification process. 3 *Biotech* **2019**, *9*, 429. https://doi.org/10.1007/s13205-019-1963-6.
- 66. Mihankhah, T.; Delnavaz, M.; Khaligh, N.G. Application of TiO 2 nanoparticles for eco-friendly biodiesel production from waste olive oil. *Int. J. Green Energy* **2018**, *15*, 69–75. https://doi.org/10.1080/15435075.2018.1423975.
- 67. Changmai, B.; Vanlalveni, C.; Ingle, A.P.; Bhagat, R.; Rokhum, S.L. Widely used catalysts in biodiesel production: A review. *RSC Adv.* **2020**, *10*, 41625–41679. https://doi.org/10.1039/D0RA07931F.
- 68. Jayaraman, J.; Alagu, K.; Appavu, P.; Joy, N.; Jayaram, P.; Mariadoss, A. Enzymatic production of biodiesel using lipase catalyst and testing of an unmodified compression ignition engine using its blends with diesel. *Renew. Energy* **2020**, *145*, 399–407. https://doi.org/10.1016/j.renene.2019.06.061.
- 69. *ASTM D6751*; Specification for Biodiesel Fuel Blend Stock (B100) for Middle Distillate Fuels. ASTM International: Conshohocken, PA, USA, 2020.
- 70. Giakoumis, E.G.; Sarakatsanis, C.K. Estimation of biodiesel cetane number, density, kinematic viscosity and heating values from its fatty acid weight composition. *Fuel* **2018**, 222, 574–585. https://doi.org/10.1016/j.fuel.2018.02.187.
- 71. *EN 14213:2003*; Heating Fuels—Fatty Acid Methyl Esters (FAME)—Requirements and Test Methods. European Committee for Standardization (CEN): Brussels, Belgium, 2003.
- 72. Rashid, U.; Anwar, F.; Knothe, G. Evaluation of biodiesel obtained from cottonseed oil. *Fuel Process. Technol.* **2009**, *90*, 1157–1163. https://doi.org/10.1016/j.fuproc.2009.05.016.
- 73. Abdalla, I.E. Experimental studies for the thermo-physiochemical properties of Biodiesel and its blends and the performance of such fuels in a Compression Ignition Engine. *Fuel* **2018**, 212, 638–655. https://doi.org/10.1016/j.fuel.2017.10.064.
- 74. Saini, P.; Gupta, C.; Shankar, R. Characterization of corn oil biodiesel and its application in diesel engine. *Energy Sources, Part A Recover. Util. Environ. Eff.* **2023**, 45, 9498–9512. https://doi.org/10.1080/15567036.2019.1679913.
- 75. Kiprono, J.; Rutto, H.; Seodigeng, T.; Enweremadu, C. Biodiesel Production Using Calcined Phosphate Rock as a Precursor of Calcium Oxide Heterogeneous Catalyst. *Environ. Clim. Technol.* **2022**, *26*, 968–981. https://doi.org/10.2478/rtuect-2022-0073.
- 76. Alptekin, E.; Canakci, M.; Sanli, H. Biodiesel production from vegetable oil and waste animal fats in a pilot plant. *Waste Manag.* **2014**, *34*, 2146–2154. https://doi.org/10.1016/j.wasman.2014.07.019.
- 77. Bandem Adnyana, I.W.; Suaniti, N.M. Ultimate analysis and acid value of biodiesel from waste oil and ethanol. *IOP Conf. Ser. Mater. Sci. Eng.* **2019**, 508, 012097. https://doi.org/10.1088/1757-899X/508/1/012097.
- 78. Oueda, N.; Bonzi-Coulibaly, Y.L.; Ouedraogo, I.W.K. Deactivation Processes, Regeneration Conditions and Reusability Performance of CaO or MgO Based Catalysts Used for Biodiesel Production—A Review. *Mater. Sci. Appl.* **2017**, *8*, 94–122. https://doi.org/10.4236/msa.2017.81007.
- 79. Gholami, A.; Pourfayaz, F.; Rodygin, K. Reusable chemical catalysts for sustainable biodiesel production: The role of metallic elements. *ChemBioEng Rev.* **2025**, *12*, e202400033. https://doi.org/10.1002/cben.202400033.
- 80. Verma, P.; Sharma, M.P. Review of process parameters for biodiesel production from different feedstocks. *Renew. Sustain. Energy Rev.* **2016**, *62*, 1063–1071. https://doi.org/10.1016/j.rser.2016.04.054.
- 81. Di Serio, M.; Tesser, R.; Casale, L.; D'Angelo, A.; Trifuoggi, M.; Santacesaria, E. Heterogeneous Catalysis in Biodiesel Production: The Influence of Leaching. *Top. Catal.* **2010**, *53*, 811–819. https://doi.org/10.1007/s11244-010-9467-y.

Disclaimer/Publisher's Note: The statements, opinions and data contained in all publications are solely those of the individual author(s) and contributor(s) and not of MDPI and/or the editor(s). MDPI and/or the editor(s) disclaim responsibility for any injury to people or property resulting from any ideas, methods, instructions or products referred to in the content.